Density Evolution After Shock Release from Laser-Driven Polystyrene Targets in Inertial Confinement Fusion

A. Shvydky,[1] D. Haberberger,[1] A. V. Maximov,[1] R. Boni,[1] D. Cao,[1] J. Carroll-Nellenback,[1] D. H. Froula,[1] V. N. Goncharov,[1] S. X. Hu,[1] I. V. Igumenshchev,[1] S. T. Ivancic,[1] V. V. Karasiev,[1] J. P. Knauer,[1] P. M. Nilson,[1] P. B. Radha,[1] S. P. Regan,[1] J. R. Rygg,[1] T. C. Sangster,[1] M. D. Rosen,[2] and V. A. Smalyuk[2]

[1]Laboratory for Laser Energetics, University of Rochester
[2]Lawrence Livermore National Laboratory

In laser-driven inertial confinement fusion (ICF), a cryogenically cooled spherical shell of deuterium–tritium (DT) fuel is imploded and compressed by material ablation to form a high-areal-density confinement around a central spot where conditions for ignition are created.[1,2] At the beginning of the implosion, multiple shocks are launched into the ablator and DT-ice shell. After the shocks break out of the shell into the gas, the shell starts to accelerate inward. The density gradient at the inner part of the shell, formed by the shock release, controls the dynamics of shell deceleration and limits the final hot-spot convergence ratio and peak fuel areal density.

To have predictive capability for ICF implosions it is important that radiation-hydrodynamic codes are able to accurately simulate the density profile of the material release ahead of the high-density shell under conditions relevant to ICF implosions (zero to a few-times solid-state density, a few to tens of eV temperature, and a few to tens of megabars of pressure). It is very difficult to probe the density profile in the material released from the inner side of the DT shell because of the low opacity of DT and various complications due to geometry. While techniques are being developed for direct density measurements during a cryogenic implosion, several key questions relevant to material release can be studied using planar foils. In recent experiments[3] release plasma profiles in planar foils were measured for the first time using optical interferometry. Results indicate that material release is enhanced in experiments compared to that predicted by radiation-hydrodynamics simulation and that the low-density part of the plasma profile in the release strongly depends on conditions at the back (opposite to the laser drive) surface right before the shock breakout. A density gradient at the back surface enhances the expansion compared to that in a classical release from a sharp foil–vacuum interface. It was hypothesized[4,5] that the formation of a density gradient at the back surface prior to shock arrival is the result of an early expansion caused by coronal x-ray preheating.

In this study, the underlying mechanisms for the enhanced release observed in experiments are examined through a systematic comparison of the experiments to radiation-hydrodynamic simulation using various thermal- and radiation-transport models and opacity and equation-of-state (EOS) tables. We find that the rarefaction-wave expansion is highly sensitive to the radiation-transport model used in the simulations. When radiation transport was treated using the S_n radiation-transport method[6] the release experiments[5] were consistently explained within the framework of radiation hydrodynamics.

The shock-release experiment carried out on the OMEGA EP Laser System used a 37-μm-thick, 4-mm-diam hemispherical CH shell (to prevent parallax in line-integrated diagnostics) and was irradiated from its inner side (front side for the laser) by two ultraviolet (UV) laser beams with a wavelength of 351 nm [see Fig. 1(a)]. With a combined laser energy of 6 kJ in a 5-ns square pulse, an overlapped intensity of 3×10^{14} W/cm^2 was obtained in a 750-μm-diam eighth-order super-Gaussian spot created using distributed phase plates. The two laser beams heated the front surface of the foil, creating ~30-Mbar ablative pressure that drove an ~65-km/s shock through the foil. At about 670 ps from the start of the laser pulse, the shock broke out from the back side of the foil and formed a rarefaction wave that expanded into the vacuum. The foil started to accelerate at about 1.3 ns, the time at

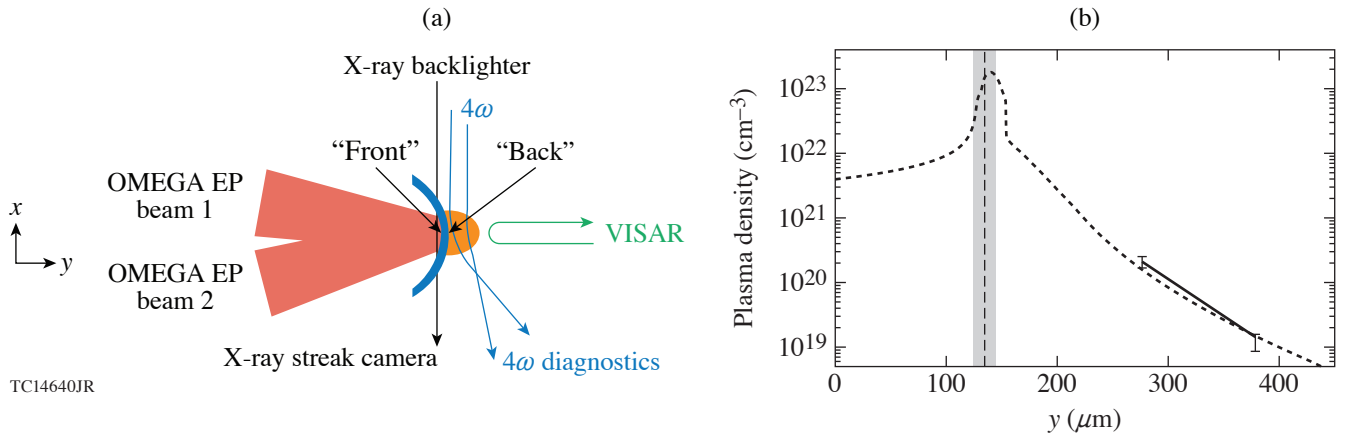

Figure 1
(a) The experimental setup used two 5-ns beams to drive a hemispherical CH shell; x-ray streaked radiography was used to measure the in-flight shell position; 4ω laser interferometry to measure the low-density profile in the rarefaction wave; and the velocity interferometry system for any reflector (VISAR) to measure the motion of the back surface of the shell. (b) The measured (solid line) and simulated (dotted curve) plasma density profiles at 2 ns. The vertical dashed line represents the peak shell positions as measured by the streak camera (with error bars shown by the shaded regions).

which the head of the rarefaction wave reached the front of the foil. The 4ω (263-nm-wavelength) interferometer[7] captured the rarefaction wave's plasma-density profile at 1, 2, 3, and 4 ns. Due to noise limitations this profile is accurate only in the low-density region measured by the 4ω probe from ~10^{19} cm^{-3} to ~10^{20} cm^{-3}; the measured density profile is further limited by the collection angle of the 4ω probe lens. As an example, Fig. 1(b) (solid line) shows the lineout of the plasma density inferred from the 2-ns interferogram taken along the middle of the drive ($x = 0$). For convenience in comparing the time evolution of the low-density part of the rarefaction wave to simulations, we extract the positions of the 10^{19}-cm^{-3} and 10^{20}-cm^{-3} plasma density locations along the middle of the drive and plot them versus time as shown in Fig. 2.

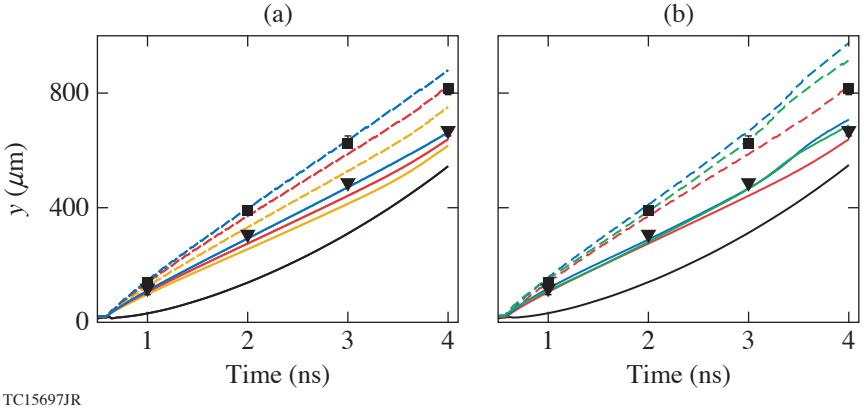

Figure 2
(a) Positions of 10^{19}-cm^{-3}-(dashed curves) and 10^{20}-cm^{-3} (solid curves) plasma density versus time from simulations performed with S_n and AOT (red), S_n and CRE (blue), and MGD and AOT (yellow); all with *SESAME* EOS. (b) Positions of 10^{19}-cm^{-3} (dashed curves) and 10^{20}-cm^{-3} (solid curves) plasma density versus time are from simulations performed with *SESAME* (red), QEOS (blue), and the ideal-gas (green) EOS; all with S_n and AOT. In (a) and (b), black squares (triangles) mark 10^{19}-cm^{-3} (10^{20}-cm^{-3}) plasma density positions and the solid black curve marks the shell trajectory.

Simulations were performed with the 1-D Lagrangian radiation-hydrodynamic code *LILAC*. The laser drive was adjusted to account for transverse thermal losses, which are not modeled in 1-D simulations, and to match the foil trajectory, which was experimentally measured and accurately simulated with the 2-D radiation-hydrodynamic code *DRACO*. An example of the simu-

lated plasma density profile taken at 2 ns is shown in Fig. 1(b) (dotted curve). The density peak (~1.8×10^{23} cm^{-3} at $y = 140$ μm) corresponds to the shell, the rising part of the density profile on the left of the shell corresponds to the corona, and the decaying part of the density profile on the right of the shell corresponds to the rarefaction wave. The simulated scale length and extent of the density profiles at all four times are in good agreement with the measurements and show a weak dependence on the opacity and EOS tables as illustrated in Fig. 2. This insensitivity indicates that radiation-hydrodynamic simulations capture essential physics in the evolution of the low-density part of the plasma profiles in the release from a CH foil into vacuum. The simulations in Fig. 2 use astrophysical opacity tables (AOT's), collisional-radiative-equilibrium (CRE) opacity tables, *SESAME* (table 7593), quotidian equation of state (QEOS), and the ideal-gas EOS models. Simulations in previous studies reported in Ref. 3, which showed much shorter expansion and scale length of the electron density profile in the release [see yellow curves in Fig. 2(a)], used a flux-limited multigroup diffusion (MGD) method[8] to model the radiation transport. MGD is the standard method for modeling radiation transport in ICF radiation-hydrodynamic codes because of its computational efficiency. The simulations shown in red, blue, and green in Fig. 2 use a more-accurate, albeit more computationally expensive, multigroup S_n radiation-transport method (method of ordinates).[6]

In summary, we have presented a consistent interpretation of the experimental results (the shock breakout time, shell trajectory, and rarefaction-wave plasma density profile) within the framework of radiation hydrodynamics: (1) The simulations showed that the low-density part of the plasma profile in the rarefaction wave formed when a shock is released from the back surface of a CH foil strongly depends on conditions at the back surface right before the shock breakout. A density gradient at the back surface enhances the expansion of the rarefaction wave compared to that in a classical release from a sharp foil–vacuum interface. When the shock travels over the low-density part of the gradient, it heats the material to higher temperatures than when the shock travels over the bulk of the shell. The higher temperature increases the sound speed of the shocked material, resulting in an enhanced release. (2) Simulations predict an early expansion (during the shock transit time) of the back surface of the foil caused by preheat by coronal x rays. Experiments using the VISAR diagnostic measured movement of the back surface of the foil during the shock transit time. The essential role of coronal x-ray preheat in the release was verified by experiments with a buried Au layer that showed a significantly reduced rarefaction-wave expansion in comparison with the baseline experiments. (3) To predict the low-density profile in the rarefaction wave, radiation-hydrodynamic simulations must accurately model preheat of the back surface of the foil by coronal x rays and the early back-surface expansion. This requires the S_n radiation transport model to accurately describe the passage of the coronal radiation through CH material under the drive conditions.

This material is based upon work supported by the Department of Energy National Nuclear Security Administration under Award Number DE-NA0003856, the University of Rochester, and the New York State Energy Research and Development Authority.

1. R. S. Craxton *et al.*, Phys. Plasmas **22**, 110501 (2015).
2. E. M. Campbell *et al.*, Matter Radiat. Extremes **2**, 37 (2017).
3. D. Haberberger *et al.*, Phys. Rev. Lett. **123**, 235001 (2019).
4. A. Shvydky *et al.*, Bull. Am. Phys. Soc. **64**, BAPS.2019.DPP.NO5.8 (2019).
5. M. D. Rosen, Bull. Am. Phys. Soc. **65**, BAPS.2020.DPP.CP17.3 (2020).
6. S. Chandrasekhar, *Radiative Transfer* (Dover Publications, New York, 1960).
7. A. Howard *et al.*, Rev. Sci. Instrum. **89**, 10B107 (2018).
8. D. Mihalas and B. Weibel-Mihalas, *Foundations of Radiation Hydrodynamics* (Oxford University Press, New York, 1984).